SEARCH FOR DARK MATTER THROUGH VERY HIGH ENERGY GAMMA-RAYS

E. MOULIN*

CEA - Saclay, DSM/IRFU/SPP,
Gif-sur-Yvette, 91191, France
**E-mail: emmanuel.moulin@cea.fr*
www.irfu.cea.fr

Annihilations of WIMPs can occur in high density regions of our Galaxy such as the Galactic Centre, dwarf galaxies and other types of substructures in Galactic haloes. High energy gamma-rays can be produced and may be detected by imaging atmospheric Cherenkov telescopes (IACTs). After a short overview of observations with current IACTs, basic principles of indirect detection through gamma-rays are given. Selected results on targeted searches such as satellites galaxies of the Milky Way are shown. In the absence of a clear signal, modelling the dark matter halo profile of these objects allows to put constraints on the particle physics parameters such as the annihilation cross section and the mass of the dark matter particle in the framework of models beyon d the Standard Model of Particle Physics. Besides theses searches are wide-field survey searches for DM substructures in the Galactic halo. The case for dark matter spikes around intermediate mass black holes will be discussed. Finally, the next generation of IACTs is presented.

Keywords: Dark matter; Gamma-rays; Cherenkov telescopes.

1. Introduction

During the last decades, compelling evidences have been accumulated suggesting a sizeable non-baryonic dark matter (DM) component in the total cosmological energy density of the Universe. The present estimate of the cold DM density is $\Omega_{\rm CDM}{\rm h}^2 \simeq 0.111 \pm 0.006$[1] where the scaled Hubble parameter is ${\rm h} = 0.70 \pm 0.02$. At the galactic scales, evidences come from the measurements of the rotation curves for spiral galaxies as well as the gravitational lensing, and agree well with the predictions of N-body simulations of gravitational clustering in the CDM cosmology. At higher scales, the velocity dispersion of galaxies in galaxy cluster suggests high mass-to-light ratio, exceeding by at least one order of magnitude the ratio in the solar neighborhood. However, almost nothing is known about the intrinsic nature of the DM particle.

Among the most widely discussed DM candidates are the WIMPs (Weakly Interacting Massive Particles). This particle can be in thermal equilibrium and in abundance in the primordial Universe. The equilibrium abundance is maintained through the annihilation with its antiparticle into lighter particles via the reaction

$\chi\bar{\chi} \rightleftharpoons l\bar{l}$. The abundance drops exponentially for non-relativistic particles as the Universe cools down. When the interaction rate becomes lower than the expansion rate, the interactions are not frequent enough to maintain the equilibrium abundance. At a given temperature, the equilibrium freeze-out and a relic cosmological abundance freezes in. The relic density is given by[2]

$$\Omega_\chi h^2 \simeq \frac{3 \times 10^{-27}\ \mathrm{cm^3 s^{-1}}}{\langle \sigma_{ann} v \rangle}\ , \tag{1}$$

where the Hubble constant h has converged towards $\sim$0.7. $\langle ... \rangle$ indicates taking a thermal average. For gauge couplings and masses of the order of the electroweak scale, the thermal relic density of massive particles automatically fullfill the WMAP constraints on the cold DM density.

Tremendous experimental and theoretical efforts are currently at play to clarify the nature of dark matter. The detection strategies that have been devised to search for dark matter can be divided into three categories. 1) The production at accelerators is looking for missing energy, jets and high-p_T particles in long decay chains; 2) The direct detection of DM particles in the Galactic DM halo aims in observing the recoiled nuclei from WIMPs scattering off of target nuclei in large undergound detectors; 3) The indirect detection of the annihilation products of two DM particles. The quest for the identification of the dark matter is a highly multidisciplinary field from cosmology to astrophysics to particle physics. The detection of the dark matter in any one of the experimental strategies will not be sufficient to conclusively elucidate the nature of dark matter. The direct and indirect detection of the dark matter particles making up the halo of our Galaxy is unlikely to provide enough information to reveal the underlying physics models behind these particles. On the other hand, collider experiments may identify long-lived particles, weakly interacting particle but will not be able to test its cosmological stability or abundance. Only the combination of the different approaches will allow to unveil the nature of the dark matter using the complementarity between the different techniques.

The indirect detection technique may proceed through the measurement of positrons and antiprotons yields in the cosmic rays, the detection of neutrinos from the center of the Sun or the Earth or high energy gamma-rays from the WIMP annihilations in the Galactic halo or in external galaxies. All these discovery methods are searching for weak signals in overwhelming backgrounds. Indirect searches through gamma-rays may be in principle easier: 1) The propagation from the production region is not affected by significant scattering or absorption; 2) The annihilation rate depends on the square of the density making "hot spots" near high concentration of dark matter as predicted by large N-body cosmological simulations; 3) The presence of possible spectral features: no gamma-ray above the DM particle mass since no more energy than the DM particle mass per particle is released in the collision of two non-relativistic particles.

The indirect detection through gamma-ray provide three types of signals. 1) A continuum of gamma-rays with a cut-off at the DM particle mass is ob-

tained via the hadronisation and/or decays of the cascading products, mainly via $\chi\chi \rightarrow q\bar{q}, W^+W^-, ... \rightarrow \gamma + ...$; 2) mono-energetic gamma-ray lines at the DM particle mass. These monoenergetic lines are produced via the reactions $\chi\chi \rightarrow \gamma\gamma$ and $\chi\chi \rightarrow \gamma Z$. The monoenergetic gamma-ray line provides an unique signature although challenging to detect because these processes are highly suppressed, i.e. gamma-rays are produced via loop-induced processes. 3) When charged annihilation products are present, an additional photon appears in the final state via radiative corrections (internal bremsstrahlung). These photons dominate at high energies and bump-like structure is present slightly lower than the DM particle mass.

2. Observations With IACTs

2.1. *The Imaging Atmospheric Cherenkov technique*

High energy gamma-rays ($E_\gamma \gtrsim 100$ GeV) penetrating in the Earth's upper atmosphere initiate electromagnetic showers via the production of electron-positron pairs and subsequent bremsstrahlung. For 1 TeV gamma-ray, the maximum development of the shower occurs at a depth of about 300 g.cm^{-2} which corresponds to an altitude of 10 km above sea level (a.s.l.) for vertical incident gamma-ray. The energy threshold for electrons and positrons to emit Cherenkov light is $\sim$40 MeV at 10 km a.s.l. The yield of Cherenkov light is proportional to the total track length of all particles, and thus proportional to the primary gamma-ray energy. An image of the cascade provides a pseudo-calorimteric measurement of the shower energy. The Cherenkov light opening angle is $\sim1^\circ$ in air and the photons produced around the shower maximum arrive at observation heights of $\sim$2000 m a.s.l. in a 120 m radius light pool. The photoelectron density is $\sim$100 per m^2 per TeV. Given the typical instrumental efficiency of 10% (reflectivity of mirror and quantum efficiency of photomultipliers) 100 m^2 optical reflector are required to obtain $\sim$100 photoelectrons in the shower image for 100 GeV gamma-ray. The Cherenkov light flash lasts a few nanoseconds and fast photomultipliers and electronics are needed to extract this faint signal over the night sky background light.

2.2. *Background rejection*

Cherenkov technique faces to the challenge of the overwhelming background from showers initiated by cosmic ray protons and nuclei. For instance, the gamma-ray rate for the brightest objects detected by HESS is only $\sim$0.1% of the background showers rate. Showers initiated by TeV protons and nuclei differ in many respects from gamma-ray showers. Most of the energy is released in pions produced in the first few interactions. The neutral pions decay produces electromagnetic sub-showers with charged pions decaying into muons. Single muons reaching the ground produce rings when impacting the telescope dish, or arcs at larger impact distances. The sub-showers generally produce substructures in the shower image and showers are generally wider than those of gamma-rays because of the the larger transverse angular

momentum implied by hadronic interactions. Moreover, for a given primary energy, hadronic interactions produce less Cherenkov light (2 to 3 times less at ∼1 TeV) due to the energy released in neutrinos, high energy muons and hadrons in the shower core. The discrimination between hadron and gamma-ray induced showers relies on the width of the shower image. Measurement and geometric parametrization of the image allow for an efficient background rejection.[3] Since then, more sophisticated methods for background rejection and shower reconstruction have been developed.[4]

2.3. *Using stereoscopy*

Multiple view of individual air shower is very useful as first demonstrated by the HEGRA collaboration.[5] A multi-telescope trigger system removes the majority of muons and hadrons initiated showers. At the analysis level, the stereoscopy improves the reconstruction of the direction and energy of the primary gamma-ray. Although the shower axis reconstruction is possible with a single Cherenkov telescope, the multiple view of the shower allows for a more accurate reconstruction of the shower direction using the intersection of the directions of the major axes of the images recorded in the cameras. The shower core location can also be better determined, thus improving the energy resolution. A better hadronic rejection is also obtained thanks to an improved shower geometry. The rejection parameter width can be replaced by mean scaled width, normalising based on expectations for gamma-ray showers (for a given image amplitude and impact distance) and averaged over all telescopes. In a Cherenkov telescope array, the optimal separation of telescopes seems to be close to the radius of the Cherenkov light-pool. Low-energy performances can be improved with closer spacing at the expense of effective collection area at higher energies.

2.4. *Current instruments*

Following the successes of the Imaging Cherenkov technique pioneered by the 10 m Whipple telescope with the discovery of the TeV emission from the Crab nebula in 1989, the ground-based Cherenkov telescopes establish a new astronomical domain with the firm detection of few tenth of sources. The ongoing generation of IACTs are relatively small field-of-view instruments (few degrees) and a duty cycle of 10% is imposed by the need of good weather and complete darkness. Best IACTs reach angular and energy resolutions of ∼0.1° and 15% respectively. Experiments are located both in Southern and Northern hemispheres allowing simultaneous and complementary observations of TeV sources. Table 1 summarises the main characteristics of currently operating major IACTs. H.E.S.S. (High Energy Stereoscopic System)[6] is a four telescope array located in the Khomas highlands of Namibia at an altitude of 1800 m above sea level (a.s.l.), completed in early 2004. Each telescope of 13 m in diameter consists of an optical reflector of 107 m^2. Each camera is equipped with 960 photomultiplier tubes (PMTs). The latitude of H.E.S.S. and the combination of a wide field of view, very good angular resolution and off-axis

Table 1. Main characteristics of currently operating IACTs. The energy threshold is given at the trigger level for observations close to the zenith. The approximate sensitivity is expressed in terms of a percentage of the flux of the Crab Nebula ($\sim 2\times10^{-11}$ cm^{-2}s^{-1} above 1 TeV) as the minimum flux of a point-like source detectable at the 5σ level in a 50 hours observation time.

Instrument	l (deg.)	b (deg.)	Alt. (m)	# of telescopes	Telescope area (m^2)	Pixels /camera	FoV (deg.)	Threshold (GeV)	Sensitivity (% Crab)
H.E.S.S.	-23	16	1800	4	107	960	5	100	0.7
MAGIC	29	18	2225	1	234	574[b]	3.5	60	2
VERITAS	32	-111	1275	4	106	499	3.5	60	2
CANGAROO-III	-31	137	160	3	57.3	427	4	400	15

Note: [a]A second telescope has recently being completed. The sensitivity is expected to be improved by a factor of $\sim$3 with the stereo operation.[b] This instrument has pixels with different sizes.

performances makes this instrument has reached an unprecedented sensitivity to accurately map the Galactic plane. VERITAS (Very Energetic Radiation Imaging Telescope Array System)[7] is an array completed recently (April 2007) and situated at the base-camp of the Whipple Observa- tory in Arizona at 1275 m a.s.l. Each telescope of 12 m diameter is composed a camera with 499 PMTs. It is similar to H.E.S.S. in several aspects and can be considered as a complementary northern hemisphere instrument. The MAGIC telescope[8] of 17 m in diameter and a mirror surface of 236 m^2, is located on the Canary island of La Palma at 2225 m a.s.l and is considered as the state-of-the-art in terms of single dish instruments. The camera contains 574 PMTs. The instrument is optimised for low energy measurements as requested for indirect DM searches. Its design has also be driven by the requirement to rapidly slew ($\sim5^\circ$/s) in case of GRB alerts. The CANGAROO-III (Collaboration of Australia and Nippon for a Gamma Ray Observa- tory in the Outback)[9] instrument has been completed in 2004. It is a system of four 10 m diameter telescopes continuing the CANGAROO project on a site near Woomera, Australia, at 160 m a.s.l. Each telescope has a surface of 75 m^2 and is equipped with a camera of 427 PMTs. Some controversy on the detection of certain sources with CANGAROO-II are now obsolete with the more sensitive observations of CANGAROO-III.

3. Gamma-Ray Flux From Dark Matter Annihilations

The gamma-ray flux expected from the annihilations of DM particles of mass $m_{\rm DM}$ accumulating in a spherical DM halo can be factored out in an astrophysical term and a particle physics term as:

$$\frac{d\Phi(\Delta\Omega, E_\gamma)}{dE_\gamma} = \frac{1}{8\pi} \underbrace{\frac{\langle\sigma v\rangle}{m_\chi^2} \frac{dN_\gamma}{dE_\gamma}}_{Particle\ Physics} \times \underbrace{\bar{J}(\Delta\Omega)\Delta\Omega}_{Astrophysics} . \quad (2)$$

The particle physics part contains $\langle\sigma v\rangle$, the velocity-weighted annihilation cross section, and dN_γ/dE_γ, the differential gamma-ray spectrum summed over the whole final states with their corresponding branching ratios. The astrophysical factor cor-

responds to the integral over the line of sight (l.o.s) of the squared density averaged over the solid angle $\Delta\Omega$ in the direction ψ, and is defined by:

$$\bar{J}(\psi, \Delta\Omega) = \frac{1}{\Delta\Omega} \int_{\Delta\Omega} d\Omega \int_{l.o.s} ds \rho^2(r(s, \psi)) \, . \tag{3}$$

For observations pointed on the target position, $\mathrm{r} = \sqrt{\mathrm{s}^2 + \mathrm{s}_0^2 - 2\mathrm{s}\mathrm{s}_0\cos\theta}$ where s_0 is the distance of the source from the Sun, and $\mathrm{d}\Omega = \sin\theta \mathrm{d}\theta \mathrm{d}\phi$. The integral along the l.o.s is calculated over the interval $\mathrm{s}_{\mathrm{min}}^{\mathrm{max}} = \mathrm{s}_0\cos\theta \pm \sqrt{\mathrm{r}_\mathrm{t}^2 - \mathrm{s}_0^2 \sin^2\theta}$. For a point-like search, $\Delta\Omega$ is usually taken to 10^{-5} sr.

3.1. *Dark matter halo modeling*

Numerical simulations are generically used to tackle the problem of large scale structure formation. Latest numerical simulations suggest the existence of an universal DM profile with the same shape for all masses and epochs[a]. One of the primeval parametrisation is the so-called NFW (Navarro, Frenk and White) profile[10] given by:

$$\rho_{\mathrm{NFW}}(r) = \rho_0 \left(\frac{r}{r_\mathrm{s}}\right)^{-1} \left(1 + \frac{r}{r_\mathrm{s}}\right)^{-2} \tag{4}$$

The normalisation parameter ρ_s, and the scale radius r_s, can be related to the virial mass and the concentration parameter using the following relations

$$\rho_0 = \frac{M_{\mathrm{vir}}}{4\pi r_\mathrm{s}^3 f(c_{\mathrm{vir}})} \quad , \quad r_\mathrm{s} = \frac{R_{\mathrm{vir}}}{c_{\mathrm{vir}}} \; ; \tag{5}$$

while the function $f(x)$ is the volume integral of the NFW profile $\mathrm{f(x)} \equiv \ln(1+\mathrm{x})$-$\mathrm{x}/(1+\mathrm{x})$ with $x = r/r_\mathrm{s}$. The virial mass is related to the virial radius by

$$M_{\mathrm{vir}} = \frac{4\pi}{3} \rho_\mathrm{u} R_{\mathrm{vir}}^3 \, . \tag{6}$$

M_{vir} is defined as the mass inside the radius $\mathrm{R_{vir}}$ with ρ_u the mean density in the Universe[b]. The NFW profile can be equally describe by given the couple of two non-degenerated parameters (ρ_s,r_s) or (M_{vir},c_{vir}). However, the numerical simulations have finite resolution and the extrapolation of the cuspy profiles toward the center of galaxies may be subject to caution with respect to the flat cores observed in astrophysical systems. On a galactic scale, a core profile is often used. The analytical expression is given by:

$$\rho_{\mathrm{Core}}(r) = \frac{v_a^2}{4\pi G} \frac{3r_c^2 + r^2}{(r_c^2 + r^2)^2} \tag{7}$$

with r_c the core radius and the v_a is the velocity scale.

[a]It is important to note that the exact value of the power-law index of the profile shape in the inner part of galaxies is still subject to debate.

[b]$\rho_\mathrm{u} = 200 \times \rho_\mathrm{c}$, with ρ_c the critical density of the universe.[11]

The determination of the free parameters of the NFW and Core profiles is done by fitting to observational data on the astrophysical object using the Jeans equation. For a spherical galaxy, the enclosed in a given radius r, $M(r)$, is related to observables by:

$$M(r) = -\frac{r\langle v_r\rangle^2}{G}\Big(\frac{\mathrm{dlog}\nu}{\mathrm{dlog}r} + \frac{\mathrm{dlog}\langle v_r^2\rangle}{\mathrm{dlog}r} + 2\beta\Big)\,, \tag{8}$$

where ν is the luminosity density, $\langle v_r^2\rangle$ is the radial velocity dispersion of the stars and β is the velocity anisotropy parameter of the stars. This method is applied in.[12]

3.2. *Exclusion limit calculation*

In the absence of a clear signal, one can compute the minimum detectable velocity-weighted annihilation cross section $\langle\sigma v\rangle_{\rm min}$ with the relation

$$\langle\sigma v\rangle_{\rm min}^{95\%\,\rm C.L.} = \frac{8\pi}{T_{\rm obs}}\frac{m_{\rm DM}^2}{\bar{J}(\Delta\Omega)\Delta\Omega}\frac{N_\gamma^{95\%\,\rm C.L.}}{\displaystyle\int_0^{m_{\rm DM}} A_{\rm eff}(E_\gamma)\frac{dN_\gamma}{dE_\gamma}dE_\gamma}\,, \tag{9}$$

where m_χ is the DM particle mass, dN_γ/dE_γ is the differential continuum photon spectrum, and $A_{\rm eff}$ is the effective area of the instrument during the observations.

In general MSSM, the continuum spectrum from neutralino annhilitaion is *a priori* not known since the branching ratios of the annihilation channels are not uniquely determined. The parametrization for a Higgsino-like neutralino annihilating mainly via W and Z bosons pairs can be computed with the parametrization from.[13] In some specific scenarios, the branching ratios of the annihilation channels can be computed given that the field content of the DM particle is known. The other popular DM candidate arises in theories with universal extra dimensions (UED). In Kaluza-Klein scenarios with KK-parity conservation, the lightest KK particle (LKP) is stable. Most often, the LKP is the first KK mode of the hypercharge gauge boson. In this case, LKP pairs annihilate mainly into fermion pairs: 35% in quark pairs and 59% in charged lepton pairs.[14]

4. Targeted Searches

4.1. *The Galactic Center*

Since 2004, H.E.S.S. observations towards the Galactic Centre have revealed a bright pointlike gamma-ray source, HESS J1745- 290,[15] coincident in position with the supermassive black hole Sgr A*, with a size lower than 15 pc. Diffuse emission along the Galactic plane has also been detected[16] and correlates well with the mass density of molecular clouds from the Central Molecular Zone, as traced by CS emission. From 2004 data set, the energy spectrum of the source is well fitted in the energy range 160 GeV - 30 TeV to a power-law spectrum with a spectral index of $2.25\pm0.04_{\rm stat.}\pm0.1_{\rm syst.}$. No deviation from a power-law is observed leading to an upper limit on the energy cut-off of 9 TeV (95% C.L.). According to

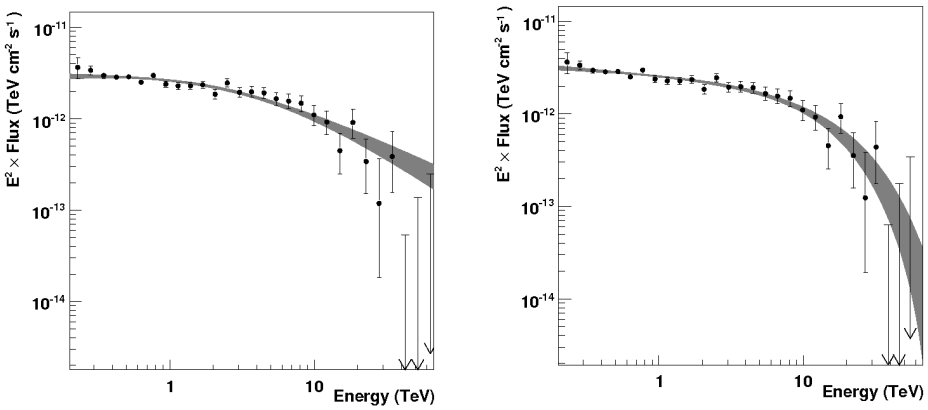

Fig. 1. HESS J1745-290 spectra derived for the 2004-2006 H.E.S.S. Galactic Centre dataset. The shaded areas are the 1σ condence intervals for the power law with an exponential cut-off fit (left) and the smoothed broken power law fit (right). The last points represent 95% condence level upper limits on the flux. Figure extracted from.[20]

recent detailed studies,[17] the source position is located at an angular distance of $7.3" \pm 8.7"_{\rm stat.} \pm 8.5"_{\rm syst.}$ from Sgr A*. The pointing accuracy allows to discard the association of the very high energy (VHE) emission with the centre of the radio emission of the supernova remnant Sgr A East but the association with the pulsar wind nebula G359.95-0.04 can not be ruled out.

The MAGIC observations were carried out towards the Galactic Centre since 2004 and revealed a strong emission[18] . The observed excess in the direction of the GC has a significance of 7.3σ and is compatible with a pointlike source. Large zenith observation angle ($\gtrsim 60^\circ$) implies an energy threshold of $\sim$400 GeV. The source position and the flux level are consistent with the measurement of HESS within errors. The differential flux can be well described by a power law of index of $2.2 \pm 0.2_{\rm stat.} \pm 0.2_{\rm syst.}$. The flux level is steady within errors in the time-scales explored within these observations, as well as in the two year time-span between the MAGIC and HESS observations.

Besides plausible astrophysical origins (see e.g.[19] and references therein), an alternative explanation is the annihilation of DM in the central cusp of our Galaxy. The spectrum of HESS J1745-290 shows no indication for gamma-ray lines. The observed gamma-ray flux may also result from secondaries of DM annihilation. The hypothesis that the spectrum measured by H.E.S.S. originates only from DM particle annihilations is highly disfavored.[15] Plausible astrophysical emitters may account for the observed signal even if a DM signal cannot be excluded. If a DM signal exists it is certainly overwhelmed by the astrophysical signals.

Various mechanisms have been suggested to explain the astrophysical GC emission over the broadband spectrum. The stochastic acceleration of electrons interact-

ing with the turbulent magnetic field in the vicinity of Sgr A*[21] would explain the millimeter and sub-millimeter emission. In this model, the IR and X-ray flaring[22] is also reproduced. It assumes in addition that charged particles are accreted onto the black hole and predicts the escape of protons from the accretion disk and their acceleration. Neutral pions are produced by inelastic collisions with the interstellar medium in the central star cluster of the Galaxy. The energy cut-off in the gamma-ray spectrum could reect an energy cut-off in the primary proton spectrum. In that case, a cut-off in the gamma-ray spectral shape at $E_{cut} \sim E_{cut,p}/30$ is expected. It would then correspond to $E_{cut,p}$ of about 400 TeV. Alternatively, energy-dependent diffusion models of protons to the outside of the central few parsecs of the Milky Way[19] have been advocated. They would imply a spectral break due to the competition between the injection and the escape of protons outside the vicinity of the GC. The G359.95-0.04 pulsar wind nebulae located at 8 arcsec from Sgr A* also explains the steepening of the measured spectrum of HESS J1745-290.[23] A fraction of the TeV emission at least may be explained by an inverse Compton emission due to a population of electrons whose energies extend up to 100 TeV. This model would imply a constant flux with time since the time scale for global PWN changes is typically much longer than a few years. The absence of TeV variability suggests that the emission mechanisms and emission regions differ from those invoked for the variable IR and X-ray emission. The models mentioned above can both accomodate a cut-off in the gamma-ray energy spectrum and predict the absence of variability in the TeV emission.

4.2. *Observations of galaxy satellites of the Milky Way*

Dwarf spheroidal galaxies in the Local Group are considered as privileged targets for DM searches since they are amongst the most extreme DM-dominated environments. Measurements of roughly constant radial velocity dispersion of stars usually imply large mass-to-luminosity ratios. Nearby dwarfs are ideal astrophysical probes of the nature of DM as they usually consist of a stellar population with no hot or warm gas, no cosmic ray population and little dust. Indeed, these systems are expected to have a low intrinsic gamma-ray emission. This is in contrast with the Galactic Centre where disentangling the dominant astrophysical signal from possible more exotic one is very challenging. Observation campaigns by IACTs have started on dwarf galaxies for a few years.[12,24–27]

The Sagittarius (Sgr) dwarf galaxy is located at $\sim$24 kpc from the Sun and is one of the nearest Galaxy satellites of the Local Group. Sgr has been observed by H.E.S.S. since 2006.[12] No significant gamma-ray excess is detected at the nominal target position. A 95% C.L. upper limit on the gamma-ray flux from standard astrophysical emission is derived: $\Phi_\gamma^{95\%\mathrm{C.L.}}(E_\gamma > 250\mathrm{GeV}) = 3.6 \times 10^{-12}\mathrm{cm}^{-2}\mathrm{s}^{-1}$ assuming a power-law spectrum of spectral index of 2.2. Sgr has made at least ten Milky Way crossings it should thus contain a substantial amount of DM to avoid to have been entirely disrupted. However, the DM halo modelling is even more

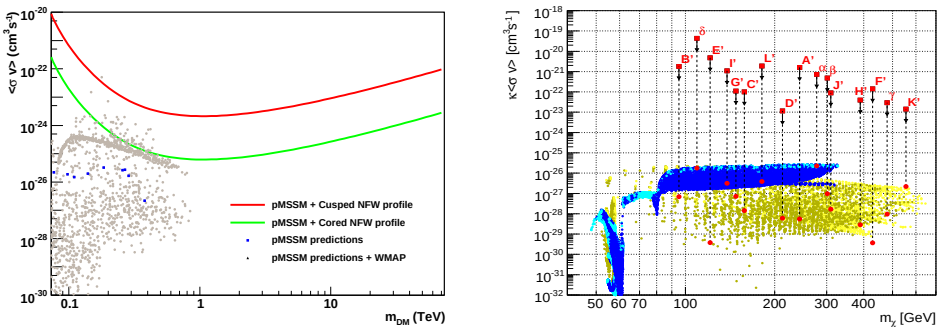

Fig. 2. Left: Upper limits at 95%C.L. on σv versus the neutralino mass for a cusped NFW and core DM halo profile for Sgr. The predictions in pMSSM are also plotted with in addition those satisfying the WMAP constraints on the cold DM density. Right: Predictions for mSUGRA models on the thermally averaged neutralino annihilation cross section as a function of the neutralino mass. Benchmarks models are plotted (red dots). The red boxes indicate the flux upper limit. See text for more details.[24]

difficult. Two models of the mass distribution for the DM halo have been studied: a cusped NFW profile and a core isothermal profile, to emcompass a large class of plausible halo profiles. The left hand side of Fig. 2 presents the constraints on the velocity-weighted annihilation cross section σv for a cusped NFW and cored profiles in the solid angle integration region $\Delta\Omega = 2 \times 10^{-5}$ sr, for neutralino DM. Predictions for SUSY models are displayed. For a cusped NFW profile, H.E.S.S. does not set severe constraints on σv . For a core profile, due to a higher central density, stronger constraints are derived and some pMSSM models can be excluded in the upper part of the scanned region.

The star velocity dispersions in Draco reveal that this object is dominated by DM on all spatial scales and provide robust bounds on its DM profile. Reduced tidal effects from the Milky Way are expected compared to Sgr. This decreases uncertainties on the astrophysical factor. The MAGIC collaboration searched for a steady gamma-ray emission from the direction of Draco.[24] The analysis energy threshold after cuts is 140 GeV. No significant excess is found. For a power law with spectral index of 1.5, typical for a DM annihilation spectrum, and assuming a pointlike source, the 2σ upper limit is $\Phi_\gamma(\mathrm{E}_\gamma > 140\mathrm{GeV}) = 1.1\times10^{-11}\mathrm{cm}^{-2}\mathrm{s}^{-1}$. The measured flux upper limit is several orders of magnitude larger than predicted for the smooth DM distribution in mSUGRA models. The limit on the flux enhancement caused by high clumpy substructures or a black hole lies in the range from 10^3 to 10^9.

Recent N-body simulations of hierarchical structure formation such as Via Lactea or Aquarius reveal the presence of DM substructures in Galactic halos. Since these results are scale invariant, they may be present in the dwarf galaxy halos and may have consequences for indirect DM searches towards dwarf galaxies. For point-

like searches towards the center of dwarf satellite galaxies, the boost factor in the predicted gamma-ray flux is of a few percent. No significant enhancement w.r.t the smooth contribution is thus expected.

5. Searches For Dark Matter Clumps

The H.E.S.S. observations of the Galactic plane between 2004 and 2007 allowed for the first time to accurately map a large field of view in the TeV energy range. This survey results in a map of the Galactic plane between $\pm 3°$ in galactic latitude and from -30° to 60° in galactic longitude with respect to the Galactic Centre position. Such a map allows to pave the way for blind DM searches, i.e. for searches for which the position of the DM target is not known *a priori*. The first study of the sensitivity in a large field of view to dark matter annihilations has been performed by H.E.S.S..[28] Fig. 4 shows the experimentally observed sensitivity map in the Galactic plane from galactic longitudes l=-30° to l=+60° and galactic latitudes b=-3° to b=+3°, for a DM particle of 500 GeV mass annihilating with 100% BR into $b\bar{b}$.

Mini-spikes around Intermediate Mass Black Holes have been recently proposed as promising targets for indirect dark matter detection.[29] The growth of massive black holes inevitably affects the surrounding DM distribution. The profile of the final DM overdensity, called mini-spike, depends on the initial distribution of DM, but also on astrophysical processes such as gravitational scattering of stars and mergers. Ignoring astrophysical effects, and assuming adiabatic growth of the black hole, if

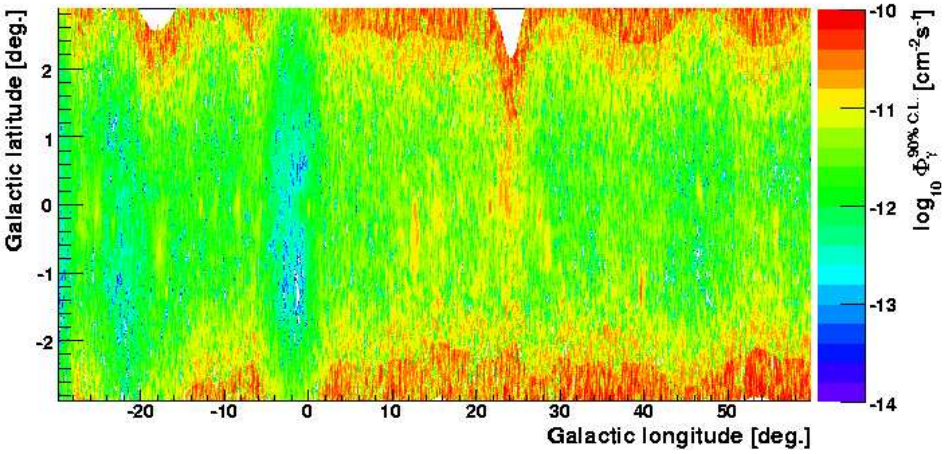

Fig. 3. H.E.S.S. sensitivity map in Galactic coordinates, i.e. 90% C.L. limit on the integrated gamma-ray flux above 100 GeV, for DMr annihilation assuming a DM particle of 500 GeV mass and annihilation into the $b\bar{b}$ channel. The flux sensitivity is correlated to the exposure and acceptance maps.

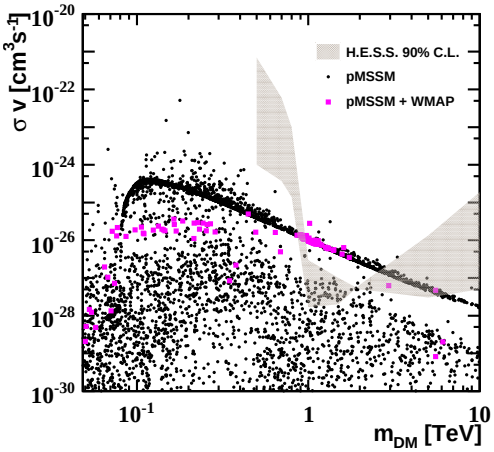

Fig. 4. Constraints at 90% C.L. on the IMBH gamma-ray production scenario for different neutralino parameters, shown as upper limits on σv as a function of the mass of the neutralino m_{DM} (grey shaded area). See Ref.[28] for more details. The DM particle is assumed to be a neutralino annihilating into $b\bar{b}$ and $\tau^+\tau^-$ pairs to encompass the softest and hardest annihilation spectra. The limit is derived from the H.E.S.S. flux sensitivity in the Galactic plane survey within the mini-spike scenario. SUSY models (black points) are plotted together with those satisfying the WMAP constraints on the DM particle relic density (magenta points).

one starts from a NFW profile, a spike with a power-law index 7/3 is obtained, as relevant for the astrophysical formation scenario studied here characterized by black hole masses of 10^5 $M_\odot$. Mini-spikes might be detected as bright pointlike sources by current IACTs. No IMBH candidate has been detected so far by H.E.S.S. within the survey range. Based on the absence of plausible IMBH candidates in the H.E.S.S. data, constraints are derived on the scenario B of Ref.[29] for neutralino or LKP annihilations, shown as upper limits on σv.[28] Fig. 4 shows the exclusion limit at the 90% C.L. on σv as a function of the neutralino mass. The neutralino is assumed to annihilate into $b\bar{b}$ and $\tau^+\tau^-$ with 100% BR, respectively. Predictions for SUSY models are also displayed. The limits on σv are at the level of 10^{-28} cm^{3}s^{-1} for the $b\bar{b}$ channel for neutralino masses in the TeV energy range. Limits are obtained one mini-spike scenario and constrain on the entire gamma-ray production scenario.

6. Next Generation Of Ground-Based Cherenkov Telescopes

6.1. *A large Cherenkov telescope array*

Following the success of the currently operating Cherenkov telescopes arrays, i.e. HESS, MAGIC and VERITAS, the next generation of IACTs is a result a joint effort of the IACT community to design a km^2-sized array of Cherenkov telescopes such as CTA (Cherenkov Telescope Array)[30] or AGIS (Advanced Gamma-ray Imaging

System),[31] to improve the overall capabilities of the present generation. CTA will consist of an array of a few tens to a thousand of telescopes with 2 to 3 different sizes to extend the accessible energy range both towards the low and the high energies. The use of different telescope sizes will allow to increase the energy range up to almost four orders of magnitude, from about 30 GeV up to 100 TeV, whereas arrays of identical telescopes are usually restricted to two orders of magnitude in energy. CTA should achieve an angular resolution better of a factor two to three regarding the angular resolutoin of HESS, and gain at least a factor of ten in sensitivity.

6.2. *A future view of the Galactic plane by CTA-like observatory*

The H.E.S.S. survey of the Galactic plane revealed a new population of gamma-ray sources.[32,33] Although progresses have been made in the understanding of the acceleleration processes at stake in these astrophysical objects, some of them remain unidentified. The extrapolation of the Galactic plane survey population to lower fluxes should allow to investigate the potential of CTA-like observatory. Given the increased capabilities of the future observatory, the senstivity is expected to be improved by an order of magnitude. The increased population of detected sources will allow to improve the understanding of Galactic gamma-ray sources.

The source population is modeled using the H.E.S.S. detected sources population given the latitude and longitude disctributions, the gamma-ray flux distribution, the angular distribution and the number of detected sources. An SNR-type population model is assumed with a SN rate of 10 per century, an efficiency of transferring explosion energy into kinetic energy of protons of $\sim$9% and the gamma-ray flux from π^0 decay is calculated using Ref.[34] The radial distribution of sources is extracted from.[35] An example of a future view of the Galactic plane by CTA-like observatory is shown on Fig. 5. Here, a flat exposure of 5 hours in each position of the map is assumed.

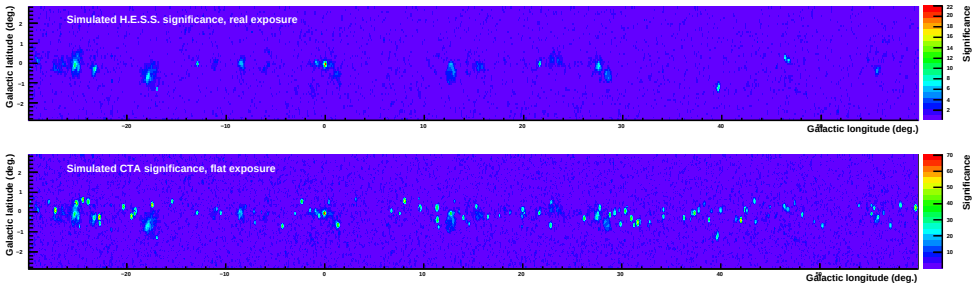

Fig. 5. A simulated view of what may be seen in the Galactic plane by a future CTA-like observatory. The upper plot shows a simulated view by H.E.S.S. using real exposure. The bottom plot is an extrapolated view for a CTA-like observatory assuming a factor 10 better in the collection area, a flat exposure of 5 hours and a background rejection improved by a factor 2, resulting in an overall factor of $\sim$10 better in sensitivity.

References

1. E. Komatsu *et al.*, *Submitted to Astrophys. J. Suppl. Ser.* (2010).
2. G. Jungman, M. Kamionkowski and K. Griest, *Phys. Rept.* **267**, 195 (1996).
3. A. M. Hillas, *Space Science Reviews* **75**, 17(January 1996).
4. M. de Naurois and L. Rolland (2009).
5. *http://www.mpi-hd.mpg.de/hfm/HEGRA/* .
6. *http://www.mpi-hd.mpg.de/hfm/HESS/* .
7. *http://veritas.sao.arizona.edu/* .
8. *http://wwwmagic.mppmu.mpg.de/* .
9. *http://icrhp9.icrr.u-tokyo.ac.jp/* .
10. J. F. Navarro, C. S. Frenk and S. D. M. White, *Astrophys. J.* **490**, 493 (1997).
11. C. Amsler *et al.*, *Phys. Lett.* **B667**, p. 1 (2008).
12. F. Aharonian *et al.*, *Astropart. Phys.* **29**, 55 (2008), Erratum-ibid.33:274,2010.
13. L. Bergstrom, *Rept. Prog. Phys.* **63**, p. 793 (2000).
14. G. Servant and T. M. P. Tait, *Nucl. Phys.* **B650**, 391 (2003).
15. F. Aharonian *et al.*, *Phys. Rev. Lett.* **97**, p. 221102 (2006).
16. F. Aharonian *et al.*, *Nature* **439**, 695 (2006).
17. *H.E.S.S. ICRC contributions* (2007).
18. J. Albert *et al.*, *Astrophys. J.* **638**, L101 (2006).
19. F. Aharonian and A. Neronov, *Astrophys. J.* **619**, 306 (2005).
20. F. Aharonian *et al.*, *Astron. Astrophys.* **503**, 817 (2009).
21. S.-M. Liu, F. Melia, V. Petrosian and M. Fatuzzo, *Astrophys. J.* **647**, 1099 (2006).
22. A. Atoyan and C. D. Dermer, *Astrophys. J.* **617**, L123 (2004).
23. J. A. Hinton and F. A. Aharonian, *Astrophys. J.* **657**, 302 (2007).
24. J. Albert *et al.*, *Astrophys. J.* **679**, 428 (2008).
25. F. Aharonian *et al.*, *Astrophys. J.* **691**, p. 175 (2009).
26. E. Aliu *et al.*, *Astrophys. J.* **697**, 1299 (2009).
27. R. G. Wagner and f. t. V. Collaboration (2009).
28. F. Aharonian *et al.*, *Phys. Rev.* **D78**, p. 072008 (2008).
29. G. Bertone, A. R. Zentner and J. Silk, *Phys. Rev.* **D72**, p. 103517 (2005).
30. *http://www.cta-observatory.org/* .
31. *http://www.agis-observatory.org/* .
32. F. Aharonian *et al.*, *Science* **307**, 1938 (2005).
33. F. Aharonian *et al.*, *Astrophys. J.* **636**, 777 (2006).
34. L. O. Drury, F. A. Aharonian and H. J. Volk, *Astron. Astrophys.* **287**, 959 (1994).
35. G. Case and D. Bhattacharya, *Astron. Astrophys. Suppl. Ser.* **120**, C437+ (1996).